JCTC Journal of Chemical Theory and Computation

Article

pubs.acs.org/JCTC

Magnesium Ion–Water Coordination and Exchange in Biomolecular Simulations

Olof Allnér, Lennart Nilsson, and Alessandra Villa*

Karolinska Institutet, Department of Biosciences and Nutrition, Center for Biosciences, SE-141 83 HUDDINGE, Sweden

ABSTRACT: Magnesium ions have an important role in the structure and folding mechanism of ribonucleic acid systems. To properly simulate these biophysical processes, the applied molecular models should reproduce, among other things, the kinetic properties of the ions in water solution. Here, we have studied the kinetics of the binding of magnesium ions with water molecules and nucleic acid systems using molecular dynamics simulation in detail. We have validated the parameters used in biomolecular force fields, such as AMBER and CHARMM, for Mg^{2+} ions and also for the biologically relevant ions Na^+, K^+, and Ca^{2+} together with three different water models (TIP3P, SPC/E, and TIP5P). The results show that Mg^{2+} ions have a slower exchange rate than Na^+, K^+, and Ca^{2+} in agreement with the experimental trend, but the simulated value underestimates the experimentally observed Mg^{2+}–water exchange rate by several orders of magnitude, irrespective of the force field and water model. A new set of parameters for Mg^{2+} was developed to reproduce the experimental kinetic data. This set also leads to better reproduction of structural data than existing models. We have applied the new parameter set to Mg^{2+} binding with a monophosphate model system and with the purine riboswitch, *add* A-riboswitch. In line with the Mg^{2+}–water results, the newly developed parameters show a better description of the structure and kinetics of the Mg^{2+}–phosphate binding than all other models. The characterization of the ion binding to the riboswitch system shows that the new parameter set does not affect the global structure of the ribonucleic acid system or the number of ions involved in direct or indirect binding. A slight decrease in the number of water-bridged contacts between A-riboswitch and the Mg^{2+} ion is observed. The results support the ability of the newly developed parameters to improve the kinetic description of the Mg^{2+} and phosphate ions and their applicability in nucleic acid simulation.

INTRODUCTION

Metal cations play a fundamental role in folding and catalysis of ribonucleic acid (RNA) systems.[1−3] RNAs are biopolymers characterized by carrying high negative charge due to their phosphodiester backbone and by forming a wide variety of complex tertiary structures with the negative phosphate groups packed close together. The negative charges work against the formation of a compact folded structure, while the presence of positive ions facilitates folding by compensating the high negative charge densities formed when the negative groups pack closely. Metal ions can bind specific sites within a folded RNA. For example, the crystal structure of the 50S ribosomal subunit shows 60 Mg^{2+} ions directly chelated by RNA, and some of them are deeply buried inside the ribosomal structure.[4] On the other hand, spectroscopic studies and thermodynamic data show that the metal ions can interact nonspecifically through water bridges with the electrostatic field generated by the RNA system.[5] These electrostatic interactions make a large contribution to the thermodynamic stability of RNA secondary and tertiary structure and also influence the kinetic mechanism of folding.[6,7]

The monovalent cations, sodium (Na^+) and potassium (K^+), and the divalent cations, magnesium (Mg^{2+}) and calcium (Ca^{2+}), influence the structure and folding of RNA in different ways. Divalent ions stabilize the RNA tertiary structure more effectively than monovalent ions. In an early work, Leroy at al. showed that the native structure of tRNA could not be achieved in a low Na^+ concentration but was restored after the addition of divalent ions.[8] Recently, Draper provided a rigorous description of the stabilization of the RNA structure by divalent ions.[9] The size of the ions also matters. Small ions, such as Mg^{2+}, are more stabilizing than larger ions such as Ba^{2+}, and the activation energy of folding is inversely proportional to ionic radii, meaning that the folding kinetics is slower with Mg^{2+} than with Ba^{2+}.[7]

Among the metal ions, Mg^{2+} ions have been shown to be the most relevant for RNA stability and folding.[10,11] Mg^{2+} ions are characterized by a high charge density due to the +2 charge and small radius (~0.65 Å). This gives the ion the ability to transfer a large amount of charge into sterically confined spaces and mitigate the negative charge of RNA structures.[4] The high charge density also results in extremely strong interactions with water molecules. Mg^{2+} forms a complex of six water molecules ($[Mg(H_2O)_6]^{+2}$) packed in an octahedral arrangement and surrounded by a second solvation shell of 12 less strongly bound water molecules.[12,13] The Mg^{2+} ion binds to RNA in two ways: directly, by replacing one of the waters in the first solvation shell with an RNA atom (inner sphere contact), or indirectly, with one of the first shell water molecules bridging between the ion and the RNA acceptor atom (outersphere contact; Figure 1).

The view that the main stabilizing contribution comes from direct binding has received less support lately, and it is now believed that the outersphere contacts are responsible for most of the stabilizing effect that Mg^{2+} ions have on RNA

Received: January 31, 2012
Published: March 12, 2012

dx.doi.org/10.1021/ct3000734 | *J. Chem. Theory Comput.* 2012, 8, 1493–1502

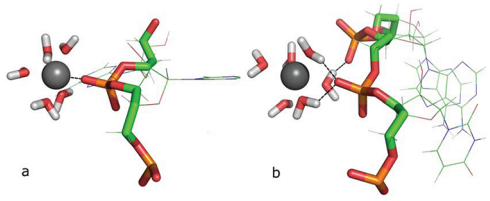

Figure 1. Examples of direct (a) and indirect (b) binding of the Mg^{2+} ion to an RNA phosphate group. Magnesium atoms are in gray, phosphor in orange, oxygen in red, carbon in green, and hydrogen in white. Picture created with Pymol, version 1.2.

structures.[14,15] The importance of indirect interactions can be attributed to the high energies (due to the partial dehydration of the $[Mg(H_2O)_6]^{+2}$ complex[5] and RNA systems[16]) required for direct binding, resulting in a very slow exchange rate of waters in the first hydration shell. This makes the energy and kinetics associated with the partial dehydration of water around the ion an important factor when predicting or modeling the binding of the Mg^{2+} ion to RNA.

Experimentally, X-ray crystallography provides structural information on the coordination of Mg^{2+} ions to RNA,[17−19] and ^{25}Mg NMR experiments[20,21] have been used to determine kinetic and thermodynamic parameters for the ion binding to RNA. These techniques provide mainly information on Mg^{2+} ions binding directly to RNA, but most of the Mg^{2+} ions bind indirectly to RNA and are hard to observe with spectroscopic methods. New emerging techniques, like anomalous small-angle X-ray scattering[22] and NMR cross-correlated relaxation rates,[23] show promising results in studying the "diffuse" ions, but still, most ion−RNA interactions remain hard to study experimentally. Computational approaches can fill in many of the voids of the experimental techniques. Poisson−Boltzmann studies have predicted Mg^{2+} induced stabilization of $tRNA^{Phe}$,[24] and recent, more advanced models have predicted Mg^{2+}−RNA binding properties.[25] Ab initito and hydrid methods have been used to assess the structure and energy contribution of Mg^{2+} binding to guanisine[26] and the guanine−cytosine base pair.[27] Classical molecular dynamics (MD) simulations have been widely used to provide directly atomistic detailed information on the dynamics and structural ion-binding feature of RNA systems.[16,28−31] For example, Auffinger and Westhof showed the sequence dependence of K^+ ion binding to nucleic acids using nanosecond atomistic simulations,[16] and recently a study by Singh et al. showed how cations are retained in major groove tunnels of an RNA molecule.[31]

The limitation of these methods lies in the accuracy of the empirical force fields and in the length of the simulation, which typically ranges up to hundreds of nanoseconds, making it impossible to directly sample the slow exchange[32,33] (on the order of microseconds) between Mg^{2+} and waters with standard simulations. Biomolecular force fields are usually parametrized using simple model systems and validated against experimental properties, and the functional forms of such force fields usually do not include polarization terms.

Metal ion parameters have been parametrized against available data for structural and thermodynamic properties in water solutions, such as the first solvation shell structure or solvation free energy.[34−36] While being an important property of ions, the calculation of solvation free energy for the metal ion in solution has been shown to be heavily dependent[37,38] on the system size and simulation conditions (i.e., long-range electrostatic descriptions). Experimentally, ion solvation free energy estimation usually relies on the free energy associated with the solvation of H^+ as a reference. Thus, published experimental scales for the ion solvation free energy can shift up and down (up to 40 kcal mol^{-1}), depending upon the chosen reference.

Here, we want to understand how the ion models reproduce the kinetic features of the ion-binding, such as activation energy or ion exchange rate, for which experimental data have become available since the initial force field parametrizations of Mg^{2+}. We will focus on the biomolecular force fields used in nucleic acid simulations (such as AMBER[39,40] and CHARMM[41,42]). Our final aim will be to achieve a reliable description of the kinetic properties of ion−RNA binding. The lack of a polarization term in the used functional form might be a limiting factor to a very accurate description for Mg^{2+} ion interactions, but we show that there is space to improve the ion description using a simple fix charge model.

The water exchange of most biologically relevant ions is too fast to be studied experimentally, but for Mg^{2+} ions, experimental data on water exchange have been published,[32,33] and kinetic parameters for magnesium binding to phosphate-containing systems are available from NMR experiments.[20,21,43]

We begin with investigating the structural and kinetic properties of ion binding from simple (ions in water solution) to more complex systems (RNA and ions in water solutions). First, we test the existing force field parameters for Na^+, K^+, Mg^{2+}, and Ca^{2+} ions, by comparing structural and kinetic properties of the aqueous ion obtained from MD simulations, with experimental data. Each ion has been simulated in explicit water solution using the TIP3P[44] water model. Then, we focus on Mg^{2+} ions, since this ion shows the greatest deviations from experimental data. We have investigated the effect of different types of water model and of different sets of ion parameters. In addition to the TIP3P water model, we have tested SPC/E,[45] another computationally cheap and widely used model in biomolecular simulations and the more complex and expensive five-site model, TIP5P.[46] We have selected the models on the basis of their different dielectric constants and/or diffusion coefficients. For magnesium ions, we have used the parameters developed by Åqvist[34] (as implemented in the AMBER99[39,40] force field) and implemented in the CHARMM27[41,42] force field. Since the observed deviation from experimental data persists with all combinations of force fields and water models, we have moved on with a reparameterization of the ion parameters. The new set of parameters for Mg^{2+} ions is optimized to fit the experimental exchange rate of the first shell water molecules.

In the second part, we focus on the interaction of Mg^{2+} ions with an isolated phosphate group and/or with the whole RNA molecule. We have investigated the effect of water and ion models on the ion−phosphate interaction. As a model system for an RNA phosphate group, we have used dimethyl phosphate (DMP) ions (see insert in Figure 5) to mimic the RNA backbone, and for modeling a biologically relevant RNA system, we have chosen the RNA purine riboswitch, *add* A-riboswitch.[47−49] The adenine riboswitch is one of the smaller natural riboswitches (71 residues), whose folding is affected by the presence of Mg^{2+} ions.[50,51] The adenine riboswitch is also a good example of intricate RNA globular folding (see Figure 2), and the X-ray structure[47] indicates a number of well-defined binding sites for the ions, *via* both inner- and outersphere contacts. We have analyzed how the hexa-hydrated ions bind to RNA, from both a structural and kinetic point of view, and

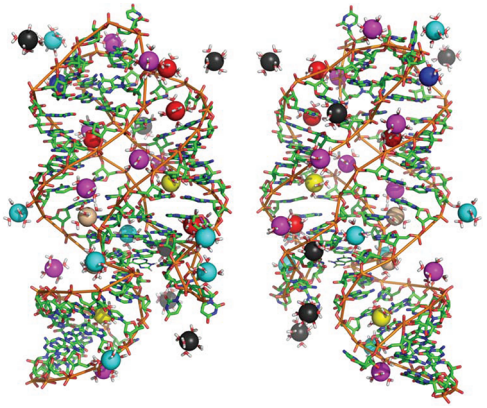

Figure 2. Snapshot of Mg^{2+} binding to *add* A-riboswitch from a MG^{NEW} simulation at 8 ns. The right projection is rotated 180° around the vertical axis. All of the ions are shown together with their first solvation shell. A selection of free ions is shown in gray. Indirectly bound ions to phosphates (in magenta); to bases (yellow);, to phosphates and sugars (in light blue); to phosphates and bases (in red); and to phosphates, sugars, and bases (in dark blue). Directly bound ions in tan. Picture created with Pymol, version 1.2.

compared the results obtained with the CHARMM27d force field.

THEORY AND METHODS

Ion−Water Interactions. Nonbonded interactions between atoms in atomistic force fields are described by an electrostatic term, expressed by a Coulombic potential, and the van der Waals term, expressed by a Lennard-Jones potential:

$$V_{\mathrm{NONBONDED}} = \sum_{\substack{\text{nonbonded}\\ \text{pairs},ij}} \left(\frac{q_i q_j}{4\pi\varepsilon_0\varepsilon_1 r_{ij}} + \varepsilon_{ij}\left[\left(\frac{R_{\min,ij}}{r_{ij}} \right)^{12} - 2\left(\frac{R_{\min,ij}}{r_{ij}} \right)^{6} \right] \right) \quad (1)$$

where i and j are all atom pair combinations within the cutoff distance, q_i is the charge of the atom i, ε_0 is the permittivity of the vacuum, ε_1 is set to 1 for explicit solvents, and r_{ij} is the distance between the atoms i and j. ε_{ij} and $R_{\min,ij}$ are the combined atomic Lennard-Jones parameters, specifying the depth (ε_{ij}) and position ($R_{\min,ij}$) of the energy minimum. ε_{ij} is obtained from the geometric mean of the two atomic parameters, $\varepsilon_{ij} = (\varepsilon_i\varepsilon_j)^{1/2}$, while $R_{\min,ij}$ is obtained from the arithmetic mean of the two atomic parameters, $R_{\min,ij} = (R_{\min,i} + R_{\min,j})/2$. The Lennard-Jones part of eq 1 can be expressed in a simplified form where the parameters have been separated into one attractive and one repulsive factor:

$$V_{\mathrm{LJ}} = \frac{C_{12}}{r^{12}} - \frac{C_6}{r^6} \quad (2)$$

where $C_{12} = \varepsilon_{ij}(R_{\min,ij})^{12}$ is the repulsive factor and $C_6 = 2\varepsilon_{ij}(R_{\min,ij})^6$ is the attractive factor.

In the reparameterization of the Mg^{2+} ion, we start from the CHARMM27[41,42] parameters (labeled as MG^{CHARMM}) and gradually modify the repulsive term (C_{12}) to fit the experimental exchange rate. This new set of parameters is labeled as MG^{NEW}.

Simulated Systems and Force Fields. *Ion−Water System.* Simulations have been performed of four ions, Mg^{2+}, Ca^{2+}, Na^+, and K^+ in water solution. Parameters implemented in the CHARMM27 force field[41,42] have been used for the metal ions and the TIP3P,[44] SPC/E,[45] and TIP5P[46] models for water molecules. The Mg^{2+} ion has also been simulated using parameters developed by Åqvist[34] and Lorentz-Berthelot-adapted to the AMBER99 force field,[39,40] labeled as $MG^{LB\text{-}Aqvist}$, and using the parameters obtained in this work.

All of the ions were centered in a rhombic dodecahedron box with 44 Å face-to-face dimensions and solvated with 1930 water molecules.

Mg^{2+}−Phosphate System. Simulations were performed on a model system of Mg^{2+} bound to a "*nucleic acid*"-type phosphate, consisting of a dimethyl phosphate (DMP) molecule in water solution. The DMP molecule was described using the CHARMM27 all-hydrogen force field.[41,42] The starting structure of the Mg^{2+} bound to one of the phosphate oxygens (O_P) was taken from the adenine-riboswitch structure (see below). The solvation box was identical to the one used for the ion−water systems.

$MgCl_2$ System. The behavior of Mg^{2+} in solution with anions was investigated by setting up and running systems (identical to the ion−water systems in all other aspects) with a neutral $MgCl_2$ solution at two ion concentrations. A 0.2 M solution was achieved with seven Mg^{2+} ions and a 1.0 M solution with 35 Mg^{2+} ions.

Adenine Riboswitch System. The complex of the *add* A-riboswitch with the purine base, adenine, was simulated in a water solution. The CHARMM27d parameters, which include an update of the 2′-hydroxyl parameters,[52] was used to describe the RNA system. As a starting structure, we used the X-ray structure of Serganov et al.[47] (PDB[53] ID 1Y26).

Hydrogen atoms were added using a standard CHARMM procedure.[54] The riboswitch complex was solvated with 10471 TIP3P water molecules in a rhombic dodecahedron box with an 80 Å face-to-face dimension. The X-ray structure includes five Mg^{2+} ions. To obtain a zero net charge of the system, we added 30 additional Mg^{2+} ions at random positions in the bulk water.

Simulation Protocols. All MD simulations were carried out using the program CHARMM36[55,56] using periodic boundary conditions. The fast lookup routines for nonbonded interactions[57] was applied when possible. The SHAKE algorithm[58] was used to constrain all bonds involving hydrogens. Newton's equations of motion were integrated using the leap-frog algorithm with a 2 fs time step. The systems were solvated with a scheme where overlapping water molecules (having the water oxygen within 2.8 Å of any solute heavy atom) were removed.

A 12 Å cutoff was used for particle−particle interactions, and the nonbonded list was constructed using a 16 Å cutoff and was heuristically updated every time an atom moved >2 Å since the last update. The long-range electrostatics were treated with the particle mesh Ewald method (PME),[59,60] a grid of 1 Å, and a κ value of 0.34. The simulations were run at constant pressure (1 atm) and temperature (298 K) using a Berendsen barostat and thermostat[61] with a coupling time of 2 ps and a compressibility of 4.63×10^{-5} atm^{-1}.

An energy minimization was made on the systems in the following way: first, 150 steepest descent (SD) and 150 adopted-basis Newton−Raphson (ABNR) steps with the solute

atoms restrained with a force constant of 15 kcal/(mol·Å^2), followed by 150 SD and 150 ABNR steps with no restraints.

The ion−water systems were simulated for 10 ns each. Convergence was assessed by dividing the trajectories into two 5 ns segments and comparing the radial distribution functions (RDFs) and the residence time of water around the ion. The residence times were found to differ <2% between the first and second half of the trajectories, and the RDFs were virtually identical in terms of shape and position of maxima and minima. The Na^+−water system was run for 40 ns for an additional verification of convergence.

To avoid structural distortions from nonoptimal positions of the Mg^{2+} ions in the adenine−riboswitch complex, the system was prepared in several steps.[62] First, energy minimizations (150 SD and 150 ABNR steps) and 200 ps of MD were performed with restraints on both RNA and ions. This procedure was then repeated two times, first, with restraints removed on ions and, finally, with all restraints removed. Finally, a 12 ns unrestrained simulation was run to equilibrate the ion positions followed by 10 ns of production time for the RNA systems.

Simulation Analyses. Radial distribution functions (RDF), $g(r)$, of water molecules around the cation were calculated from the unrestrained trajectories over 200 points with a bin size of 0.04 Å (8 Å in total). A potential of mean force (PMF) can be obtained by inverting the RDF: PMF = $-RT\ln(g(r)) + c$. The constant c can be ignored since we are only interested in the relative change in free energy.

Umbrella Sampling. Potential of mean force (PMF) profiles were calculated using umbrella sampling with the harmonic bias potential $w_i(x) = k(x - x_i)^2$ along a reaction coordinate, x, defined as the distance between the Mg^{2+} ion and the water oxygen (O_w) or the distance between Mg^{2+} and the phosphate oxygen (O_P) in the DMP system. We used a total of 53 simulation windows with the reference value for the bias potential x_i ranging from 1.6 Å to 6 Å in 0.1 Å intervals, and from 6 Å to 10 Å in 0.5 Å intervals. Initial conformations for each window were generated by running 20 ps of MD at each point along the reaction coordinate, with k = 500 kcal/(mol·Å^2), using the last structure in each window as the starting structure in the next window.

In the production phase, each window was run for 1.0 ns (of which the first 0.2 ns was equilibration time) with a force constants of k = 150 kcal/(mol·Å^2) for the first windows up to 6 Å and k = 10 kcal/(mol·Å^2) for the last windows between 6 Å and 10 Å. The PMF curves were constructed from the resulting distance distributions using the Weighted Histogram Analysis Method[63,64] with a tolerance of 10^{-5}. All of the curves have been translated to zero at a Mg^{2+}−$O_{W/P}$ distance of 8 Å for ion−O_w and 9 Å for the Mg^{2+}−O_P profiles. When the distance between the two mass centers is constrained, free rotation of the solute−solute connecting vector remains possible, and larger volume elements are sampled at larger distances. This leads to an entropic contribution, $S = 2\,RT\ln(x)$, to the average constraint force that must be subtracted out.

Error bars were obtained by dividing the trajectories of each window into three parts and calculating the standard deviation between them. For the three PMFs of Mg^{2+}−O_w using the TIP3P water model, error bars were calculated using three independent replica simulations, each with 1 ns of simulation of each point along the reaction coordinate.

Calculation of Rate Constants. Transition state theory gives a relation between the rate constant (k) and the free energy of activation, $\Delta G^{\dagger}$:

$$k = A\ e^{-\Delta G^{\dagger}/RT} \tag{3}$$

where A is a pre-exponential factor with unit s^{-1}, T is the temperature, and R is the gas constant. The prefactor describes the frequency at which a system oscillates in its minima, and the exponential factor describes the probability the oscillations have to cross the barrier of $\Delta G^{\dagger}$. To determine the pre-exponential factor, we use two approaches: (1) by directly calculating the oscillation frequency of ion−water oxygen distance in an unrestrained simulation and (2) by the second derivative of the PMF as a function of the atom pair distance at the bottom of the well according to $A = 1/2\pi(E''/\mu)^{1/2}$, where E'' is the second derivative of the PMF and μ is the reduced mass of the atom pair. The second derivative was determined by fitting a second order polynomial to the bottom data points, symmetrically centered around the minimum of the energy well. The two approaches give very similar values: 6.6×10^{12} s^{-1} vs 6.7×10^{12} s^{-1} (for Na^+−O_w), 5.0×10^{12} s^{-1} vs 5.0×10^{12} s^{-1} (for K^+−O_w), 1.4×10^{13} s^{-1} vs 1.3×10^{13} s^{-1} (for Mg^{2+}−O_w), and 9.1×10^{12} s^{-1} vs 8.9×10^{12} s^{-1} (for Ca^{2+}−O_w). The calculated values show an insignificant difference when determined from simulations using different ion parameter sets or water models (data not shown). In this work, we use the values obtained by approach 2.

The free energy of activation, $\Delta G^{\dagger}$, was estimated from the PMFs as the energy difference between the global minimum (binding distance) and the global maximum (peak of transition barrier).

The exchange rate of H_2O can also be calculated by directly counting the number of exchanges during the simulation. This approach is applicable only to those ions that have fast exchange (on the order of 10−100 ps) since the exchange time should be shorter than the simulation time to guarantee good sampling. To calculate the mean residence time, τ, of a water−ion contact, we have to define when the ion and water are in contact. For Na^+ ions, a contact was defined when the distance between the Na^+ ion and a water oxygen was within 3.1 Å. This corresponds to the position of the first peak in the PMF. The exchange rate, k, is then calculated as the inverse of the mean residence time.

Free Energy of Solvation. We have calculated the relative solvation free energy, ΔG^{REL}_{SOLV}, between a Mg^{2+} ion represented by two parameter sets, MG^{CHARMM} (state A) and MG^{NEW} (state B).

The free energy difference between the two states was calculated using the coupling parameter approach together with the thermodynamic integration:

$$\Delta G_{AB} = \int_{\lambda_A}^{\lambda_B} \left\langle \frac{\delta H(\lambda)}{\delta \lambda} \right\rangle_{\lambda_i} d\lambda_i \tag{4}$$

where the Hamiltonian (H) is a function of the coupling parameter λ, $H(\lambda) = \lambda H_B + (1-\lambda)H_A$. The coupling parameter λ defines the progress of the system along the path between the initial and final states by ranging from 0 (state A, ion−water interactions with MG^{CHARMM}) to 1 (state B, ion−water interactions with MG^{NEW}). One approach to evaluate the integral in eq 4 is to calculate the average at a number of discrete λ steps (denoted by λ_i in eq 4) between 0 and 1 by

Table 1. Structural and Kinetic Data for the Ion−Water Systems from Simulation and Experiment[a]

metal parameter	water model	$\Delta G^{\dagger}$ (kcal/mol)	k_1 (s^{-1})	r_1 (Å)	r_2 (Å)	CN_1/CN_2
			Mg^{2+}			
MG^{CHARMM}	TIP3P	12.7 ± 0.2	6.4×10^3	1.97	4.1	6/12
MG^{CHARMM}	SPC/E	12.6 ± 0.5	7.5×10^3	2.00	4.1	6/12
MG^{CHARMM}	TIP5P	13.1 ± 0.6	3.2×10^3	1.90	4.0	6/12
$MG^{LB\text{-}Åqvist}$	TIP3P	13.2 ± 0.2	2.7×10^3	1.98	4.2	6/12
MG^{NEW}	TIP3P	9.9 ± 0.1	6.8×10^5	2.04	4.2	6/12
exptl.		9.9	$6.7 \pm 0.2 \times 10^5$ [b]	2.07[c]−2.11[d]	4.1−4.2[c]	6/12[c]
			Ca^{+}			
CA^{CHARMM}	TIP3P	3.5	2.4×10^{10}	2.32	4.6	7.6/16
exptl.			$>10^{10}$ [e]	2.39−2.44[c]	4.5−4.6[c]	7/[c]
			Na^{+}			
NA^{CHARMM}	TIP3P	2.9	5.0×10^{10}	2.32	4.6	5.8/18
exptl.			$>10^{10}$ [f]	2.33−2.50[c]		5.6/[c]
			K^{+}			
K^{CHARMM}	TIP3P	1.6	4.6×10^{11}	2.71	5.1	6.5/18
exptl.			$>10^{10}$ [e]	2.6−2.8[c]		5.5/[c]

[a]Values of activation energy ($\Delta G^{\dagger}$) (together with the calculated error), the ion−water exchange rate from the first solvation shell (k_1), distances (r_1/r_2), and coordination numbers (CN_1/CN_2) to/of the first and second solvation shell are reported for Mg^{2+}, Ca^{2+}, Na^{+}, and K^{+}. For simulations, the ion parameter set and water models are also reported. Reported $\Delta G^{\dagger}$ values are the average values of three simulations, and the error intervals are the corresponding standard deviations. [b]Bleuzen et al.[33] [c]Othtaki and Radnai.[67] [d]Caminiti et al.[12] [e]Weingartner et al.[76] [f]Helm and Merbach.[68]

performing separate simulations for each of the chosen λ steps. The integral can then be determined numerically.

To calculate the free energy, we have used a dual-topology approach as implemented in the *thermodynamic simulation methods* (TSM) module of the CHARMM package.[65,66] Separate simulations were performed for 11 λ values, linearly spaced between 0 and 1. At each λ point, the system was first equilibrated for 50 ps, and then data were collected for a further 100 ps. Three independent sets of simulations have been used to calculate ΔG^{REL}_{SOLV}, and the error was determined by calculating the standard deviation between the obtained values.

RESULTS AND DISCUSSION

Ions in Water Solution. MD simulations for Na^{+}, K^{+}, Mg^{2+}, and Ca^{2+} ions have been performed in water solutions for 10 ns, using the TIP3P model for water molecules and CHARMM27 parameters for the ions. Table 1 reports the main structural parameters obtained from our simulations together with experimental values when available. The reported structural properties of ions are acquired from X-ray and neutron diffraction experiments (see review by Ohtaki and Radnai[67] for a detailed description).

We define the distances between the ion and the water molecules in the first and second coordination shells (r_1 and r_2 in Table 1) as the position of the first and second peaks in the RDF, respectively. The r_1 values lie within the range of experimental values for Na^{+} and K^{+}, or very close (a deviation from experiment values of <4%) to the experimental values for Ca^{2+}, while for Mg^{2+}, the deviation is larger (~6%). The r_2 value has a value of 4.6−5.1 Å for monovalent ions, while for the divalent ions it is 4.1−4.6 Å. The second solvation shell is not well-defined for the monovalent ions, and therefore, no experimental data are available. In case of the divalent ions, Mg^{2+} (4.1 Å) and Ca^{2+} (4.6 Å), the CHARMM parameters and TIP3P water model reproduce the experimental distances (4.1−4.2 Å for $Mg^{2+}$and 4.5−4.6 Å for Ca^{2+}) accurately. The water coordination number for the first and second solvation shell (CN_1 and CN_2) of Mg^{2+} agrees well with experimental data. As with r_2, CN_2 is not well-defined for the monovalent ions Na^{+} and K^{+}, and no experimental data are available for Ca^{2+} ions as far as we know.

Before calculating the kinetic properties of the ion−water system, we check that a simulation time of 10 ns was enough to guarantee the convergence of the water residence time around the ions. That is not the case for Mg^{2+}. For this ion, no ion−water exchanges were observed during the simulations. To obtain the kinetic parameters for the Mg^{2+}, umbrella sampling was used to generate the PMF profile between the ion and water molecules, from which the heights of activation barriers of ion−water binding were obtained. In all umbrella sampling windows, the Mg^{2+} ion is coordinated by six molecules, except in those windows corresponding to the maximum in the energy profile where the ion is coordinated by five water molecules plus two water molecules at slightly larger distances, one is the pulled water molecules and the other is a water molecule about to replace the pulled one.

Figure 3 shows the potential of mean force profile between the ion and oxygen of a water molecule for all four ions. In the case of Na^{+}, K^{+}, and Ca^{2+}, the PMF is obtained by inverting the RDF calculated between the ion and water oxygen. The values of the activation free energy, $\Delta G^{\dagger}$, are reported in Table 1. Applying eq 3, we have calculated the exchange rate for the ion−water binding (k_1 in Table 1) from $\Delta G^{\dagger}$ using the following prefactor values: (1) $Na^{+}-O_w = 6.7 \times 10^{12}$ s^{-1}, (2) $K^{+}-O_w = 5.0 \times 10^{12}$ s^{-1}, (3) $Mg^{2+}-O_w = 1.3 \times 10^{13}$ s^{-1}, and (4) $Ca^{2+}-O_w = 8.9 \times 10^{12}$ s^{-1}.

We compared the kinetic constant, k, for $Na^{+}-H_2O$ exchange calculated from $\Delta G^{\dagger}$ (using eq 3) with the rate obtained from analysis of the mean residence time of O_w in the first solvation shell of Na^{+}. Both exchange rate constants, 5.0×10^{10} s^{-1} using eq 3 and 2.52×10^{10} s^{-1} from direct counting, are in agreement with the available experimental information ($>10^{10}$ s^{-1}). In the following, the kinetic constants, k, are calculated from $\Delta G^{\dagger}$.

To compare the results with available experimental data, we have to take some considerations into account. Experimental data describing the kinetics of water exchange around ions are best acquired from ^{17}O NMR experiments,[32,33] but the limit in

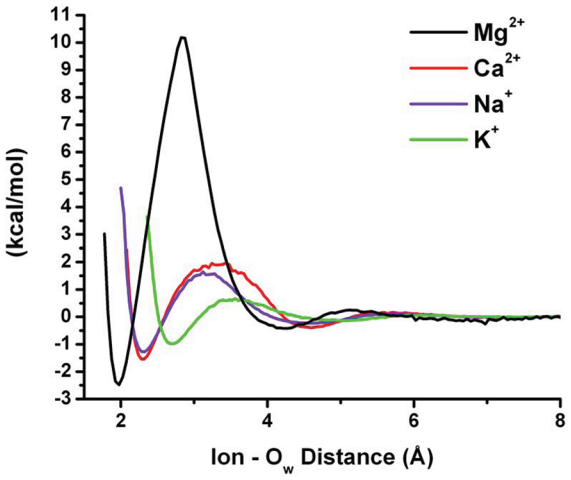

Figure 3. Potential of mean force between the ion and a water oxygen for all investigated ions. The data for Mg^{2+} have been obtained with umbrella sampling. Simulations performed using the CHARMM27 force field for ions and TIP3P as water model.

time resolution of these techniques lies at about 10^{-10} s, which is not enough to accurately measure the exchange rate (k) of water around Na^+, K^+, and Ca^{2+}. With this in mind, we can see that the rate constants, calculated from the free energy of activation for Na^+ (5.0×10^{10} s^{-1}), K^+ (3.3×10^{11} s^{-1}), and Ca^{2+} (2.4×10^{10} s^{-1}) lie within an order of magnitude from the experimental values (>10^{10} s^{-1}). We can also see that the relative values of exchange rate for these three ions, $K^+ > Na^+ > Ca^{2+}$, agree with the experimental data reported in a review by Helm and Merbach.[68] Another aspect to consider is that experimental studies[32,33] have approximated the prefactor A used in eq 3 (relating $\Delta G^{\dagger}$ with k) with $A = k_B T/h = 6.2 \times 10^{12}$ s^{-1}, while we have determined A directly from the simulation data.

The agreement between the experimental and simulated data observed for Na^+, K^+, and Ca^{2+} ions gives strength to the view that the CHARMM27 parameters and the TIP3P water model describe the structural and kinetic aspects of the binding of these ions with water molecules accurately. Mg^{2+} ions have a considerably slower exchange rate than the other three ions, both in experiments and in simulations, but the calculated exchange rate of 6.4×10^3 s^{-1} is 2 orders of magnitudes slower than the experimental rate[33] of 6.7×10^5 s^{-1}. This prompts us to find a better representation of Mg^{2+} in water solution.

Water Models. To study the effect of the water models on the structure and kinetics of Mg^{2+}–H_2O complexes, we calculated PMF-profiles of Mg^{2+} solvated with SPC/E and TIP5P water molecules in addition to TIP3P (Figure 4, Table 1). The SPC/E water model reproduces the experimental distance to the first hydration shell (r_1) slightly better (2.00 Å) than the TIP3P model but still underestimates the distance by almost 5%. The result does not improve with the TIP5P water model with an r_1 distance of only 1.90 Å, around 10% below the experimental value. The reproduction of the second hydration shell is better, with the SPC/E model producing the experimental 4.1 Å and the TIP5P model slightly below, at 4.0 Å. The coordination numbers for the two solvation shells are correctly reproduced for all three water models.

The free energy of activation, $\Delta G^{\dagger}$, calculated with different water models lies within the error margin (see Table 1). All of the barrier values give exchange rates off by more than 2 orders of magnitude from the experimental value. This points out that the difference in models does not affect the kinetic description of Mg^{2+}–H_2O interactions.

Mg^{2+} Parameter Sets. Another factor involved in the Mg^{2+}–H_2O interactions are the Lennard-Jones parameters of the metal ion. We have compared MG^{CHARMM} and $MG^{LB\text{-}Åqvist}$ with a new set of parameters, MG^{NEW} (Table 2), which has been optimized to reproduce the experimental exchange rate of water in the first solvation shell. The new Mg^{2+} Lennard-Jones potential has a significantly lower well depth (ε) than

Table 2. Lennard-Jones Parameters for Mg^{2+} from CHARMM27, Lorentz-Berthelot Adapted Åqvist and the Set Developed in This Work

	MG^{CHARMM}	$MG^{LB\text{-}Åqvist}$	MG^{NEW}
ε [kcal/mol][a]	0.015	0.8947	0.00295
R_m [Å][a]	2.37	1.5852	3.109
σ [Å][b]	2.11	1.41	2.77
C_{12} [Å^{12}·kcal/mol][c]	471.1	225	2400
C_6 [Å^6·kcal/mol][c]	5.32	28.4	5.32

[a] ε and R_m are the depth and the position of the minimum of the Lennard-Jones potential (see eq 1). [b] $\sigma = R_m/2^{1/6}$. [c] The repulsive term, $C_{12} = \varepsilon_{ij}(R_{min,ij})^{12}$, and the attractive term, $C_6 = \varepsilon_{ij}(R_{min,ij})^6$, of eq 2.

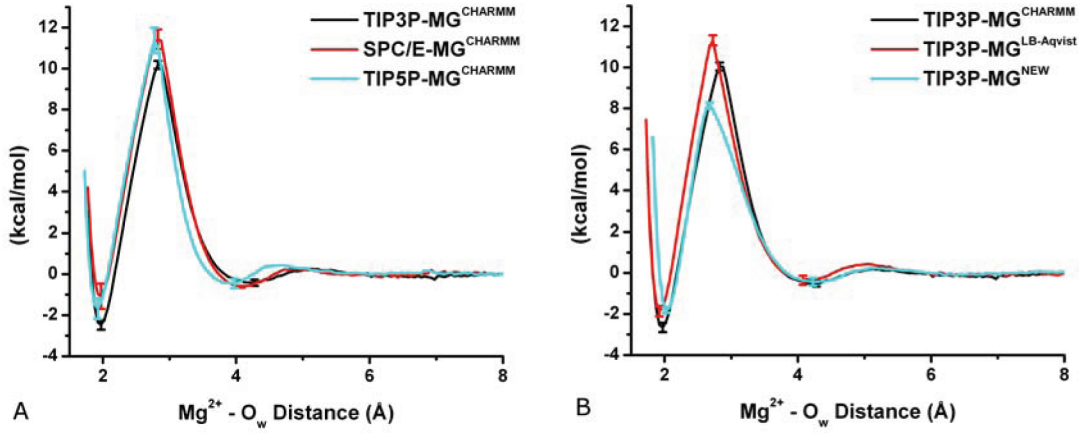

Figure 4. Potential of mean force between Mg^{2+} and a water oxygen around Mg^{2+} using different water models (a) and Mg^{2+} parameters (b). Error bars were estimated as the standard deviation from three separate simulations.

MG^{CHARMM} and $MG^{LB\text{-}Åqvist}$. However, the effect of this has little influence on the first solvation shell since the strong attractive electrostatic interactions pull the interacting atoms (Mg^{2+}–O_w, Mg^{2+}–O_P, etc.) at a distance far up on the "repulsive wall" of the Mg^{2+}–O Lennard-Jones potential, far away from the minimum.

The structural properties (Table 1) of $MG^{LB\text{-}Åqvist}$ (r_1 = 1.98 Å and r_2 = 4.2 Å) are very similar to the results using MG^{CHARMM}. With MG^{NEW}, the distance to the first solvation shell (r_1 = 2.04 Å) is improved considerably compared to all previous results, while r_2 (4.2 Å) is kept at the correct experimental value.

The comparison of PMF profiles for the three Mg^{2+} parameters (Figure 4, Table 1) shows that the $MG^{LB\text{-}Åqvist}$ parameters do not exhibit better kinetic properties than MG^{CHARMM}; the barrier ($\Delta G^{\dagger}$ = 13.2 ± 0.2 kcal/mol) gives an exchange rate nearly 3 orders of magnitudes slower than the experimental one. The MG^{NEW} parameters ($\Delta G^{\dagger}$ = 9.9 ± 0.1 kcal/mol) reproduce the experimental exchange rate (to which it has been optimized) within the error margin of the ^{17}O NMR experiment (keeping in mind that a 0.1 kcal/mol error in $\Delta G^{\dagger}$ translates into an error of around 1.5 × 10^5 s^{-1} in k).

The exchange rates of water from the second solvation shell, k_2, obtained from the second minima and barrier of the PMFs, reveal only small variations between the different water models and ion parameters, all within the error margin. The prefactor for these interactions was determined from the second energy well and is 2.14 × 10^{12} s^{-1}. The calculated exchange rates, k_2, are in the range 4.3 × 10^{11} s^{-1} to 7.3 × 10^{11} s^{-1}. No experimental data exist for these exchange rates as far as we are aware.

The reparameterization of the Mg^{2+} was performed by solely modifying the repulsive term Lennard-Jones term, C_{12}, to avoid altering the solvation properties of the ions too much. To check the effect of the new parameters on the solvation free energy value, we have calculated the relative solvation free energy between MG^{CHARMM} and MG^{NEW}. Changing the ion parameter from MG^{CHARMM} to MG^{NEW} corresponds to a change of 24.4 kcal/mol in the solvation free energy, which is less than 6% of the reference values for MG^{CHARMM} (−441.65 kcal/mol[69]) and around 6% of the experimental values (between −435.4 and −437.4 kcal/mol).[70,71] Note that MG^{CHARMM} was originally parametrized to reproduce the solvation free energy.

We have also checked that the MG^{NEW} parameters do not affect the description of an ion solution compared to the original force field. We have done this by performing a 10 ns MD simulation of $MgCl_2$ at a concentration of 0.2 and 1 M in a water solution using MG^{CHARMM} and MG^{NEW} for Mg^{2+} and compared the Mg^{2+}–Cl^- radial distribution function. Both force fields show a first peak at around 4.2 with similar height according the concentration conditions. The change in Mg^{2+} parameters does not affect the ion distribution in solution in a relevant way, and the results are in line with experimental evidence that Cl^- tends to be surrounded by its own hydration shell.[12]

Mg^{2+}–Phosphate Interactions. To model the binding between Mg^{2+} ions and nucleic acid phosphates, a system consisting of a Mg^{2+} ion and a dimethyl phosphate (DMP) in a water solution has been used. The potential of mean force between the phosphate oxygen (O_P) of DMP and the Mg^{2+} ion has been calculated using different water models and magnesium parameters (Figure 5). The Mg^{2+}–O_P minimum distance (Table 3) is shorter than the Mg^{2+}–O_W distance, due

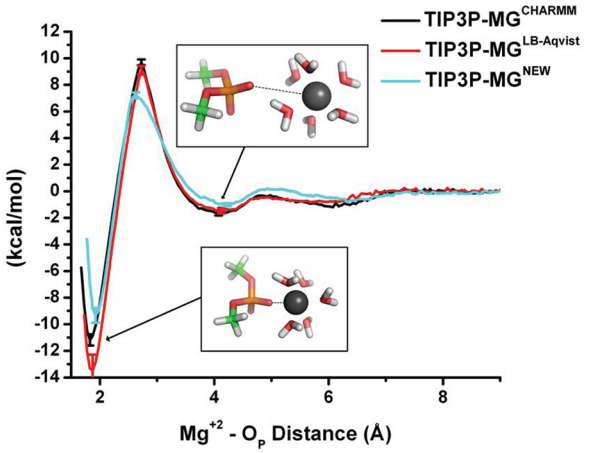

Figure 5. Potential of mean force between Mg^{2+} and the O_P of a phosphate group using different Mg^{2+} parameters. Error bars were estimated as the standard deviation from three separate simulations. Inset figures show the structure of the system at the two minima.

to the negatively charged phosphate group. Only small differences for the Mg^{2+}–P distance (Table 3) are seen between the different water models and Mg^{2+} parameters, but MG^{NEW} parameters reproduce the Mg^{2+}–P distance (calculated value of 3.41 Å vs experimental value of 3.6 Å[72]) better than the other models (3.30–3.38 Å). For the second shell interactions, the TIP5P water model stands out with an r_2 (O_P) distance considerably shorter (3.6 Å) than the other models (4.0–4.1 Å). No data on the distance between Mg^{2+} and Op atoms bridged by a water molecule are reported in the X-ray diffraction work on a magnesium–phosphate solution. Caminiti[72] in his analysis showed an average number of one phosphate bound to Mg^{2+}, indicating that the cation is always directly bound to the phosphate in his experiment.

The kinetic constants (k_1 and k_2) were calculated for both the direct (k_1) and indirect (k_2) binding of Mg^{2+} to the phosphate group (Table 3), using a prefactor calculated to be 1.1 × 10^{13} s^{-1} for the Mg^{2+}–phosphate system and 2.7 × 10^{12} for the second solvation shell. The TIP5P model gives a considerably faster rate (4.1 × 10^{-1} s^{-1}) than TIP3P and SPC/E models (2.6 × 10^{-3} s^{-1} and 1.7 × 10^{-2} s^{-1}).

A comparison of the three Mg^{2+} parameters (Figure 5 and Table 3) shows that $MG^{LB\text{-}Åqvist}$ (1.3 × 10^{-3} s^{-1}) performs similarly to MG^{CHARMM}, while the MG^{NEW} parameters give a rate (10.3 s^{-1}) that is several orders of magnitude faster. This exchange rate is far too slow to be possible to sample with any reasonable simulation times without artificial constraints. As far as we know, no experimental data are available for the phosphate– Mg^{2+} exchange in a monophosphate system like DMP. ^{25}Mg NMR studies are available for Mg^{2+}–nucleic acid systems. A value of 0.5 × 10^3 s^{-1} was reported for magnesium binding to DNA,[21] 1.5 × 10^3 s^{-1} for 5S rRNA[20] and 2.5 × 10^3 s^{-1} for $tRNA^{Phe}$.[20] The values obtained with MG^{NEW} parameters exhibit the best agreement with these experimental rates compared to the other two sets of parameters. In this comparison, we have to take into account that the experimental exchange rates may be affected by interactions between the ions and other atoms in the nucleic acid systems that are not present in our model systems.

The exchange rates of the second shell binding show smaller differences than the first shell exchange and lie between 2.0 and 4.7 × 10^{11} s^{-1} for all systems. The rates mean that these

Table 3. Structural and Kinetic Data for the Mg^{2+} Phosphate System[a]

Mg^{2+} Parameters	water model	$\Delta G_1^{\dagger}$ (kcal/mol)	k_1 (s^{-1})	$\Delta G_2^{\dagger}$ (kcal/mol)	k_2 (s^{-1})	$r_1(O_P/P)$ (Å)	$r_2(O_P)$ (Å)
MG^{CHARMM}	TIP3P	21.3 ± 0.2	2.6×10^{-3}	1.3 ± 0.07	2.8×10^{11}	1.85/3.30	4.1
MG^{CHARMM}	SPC/E	20.2 ± 0.4	1.7×10^{-2}	1.3 ± 0.06	2.8×10^{11}	1.86/3.32	4.0
MG^{CHARMM}	TIP5P	18.3 ± 0.4	4.1×10^{-1}	1.5 ± 0.09	2.0×10^{11}	1.90/3.38	3.6
$MG^{LB\text{-}Åqvist}$	TIP3P	21.7 ± 0.3	1.3×10^{-3}	1.0 ± 0.08	4.7×10^{11}	1.87/3.35	4.1
MG^{NEW}	TIP3P	16.4 ± 0.2	10.3	1.2 ± 0.05	3.4×10^{11}	1.94/3.41	4.2
exptl.		12.7−13.3	0.5×10^3 to 2.5×10^3 [c]			/3.6[b]	

[a]Values of activation energy ($\Delta G^{\dagger}$; together with the calculated error), the ion−water exchange rate (k), and distances (r) between ion and phosphate oxygen (O_P) and/or phosphorus (P) are reported. The number in the subscript refers to the first and second solvation shells. $\Delta G^{\dagger}$ values are the average values of three simulations, and the error intervals are the corresponding standard deviation. [b]Caminiti et al.,[72] [c]Cowan et al.[20,21,43]

interactions are very short-lived with residence times measured in a few picoseconds, the same order of magnitude shown by water with K^+ ions. It is noteworthy that the TIP5P water model gives a fast first shell exchange but has the slowest exchange rate from second shell binding.

Mg^{2+}−RNA Interactions. To test the performance of the MG^{NEW} parameters in a nucleic acids context, *add* A-riboswitch was simulated in explicit water/Mg^{2+} ions solution, using the MG^{CHARMM} and MG^{NEW} parameters for the ion and TIP3P model for water molecules. We used the CHARMM27d force field to describe RNA, since the MG^{NEW} was developed starting from the ion parameters implemented in the CHARMM force field. The X-ray structure[47] of the A-riboswitch includes five Mg^{2+} ions, of which two are directly bound to an RNA phosphate. Thirty additional Mg^{2+} ions had to be added to neutralize the system. First, we have checked that the use of different Mg^{2+} did not affect the tertiary structure of the RNA. Both MD simulations yielded structures similar to the experimental structure with an overall RMSD of 3.21 Å with MG^{CHARMM} and 3.01 Å for MG^{NEW}, in agreement with a previously performed simulation.[73] All of the secondary and tertiary structure elements are conserved during the 10 ns simulation. Although 10 ns simulations are too short to assess the RNA force field performance, the results suggest that the ion parameters do not lead to any gross structural distortions on this time scale. Then, the behavior of the two parameter sets has been compared by calculating the direct and indirect contacts made by Mg^{2+} ions to RNA system. Both simulations show two ions bound via innersphere contacts to the RNA system in agreement with the crystallographic structure. Among the other ions, on average 24.4 (MG^{CHARMM}) or 22.2 (MG^{NEW}) ions are bound to the riboswitch via outersphere contacts. Each outersphere contact has an average lifetime of 52 ± 2.7 ps with MG^{CHARMM} and 57 ± 5.3 ps with MG^{NEW} (average values and standard deviations obtained from five segments of 2 ns each) before breaking.

The two Mg^{2+} ions that were directly bound to RNA in the X-ray structure remain bound during the simulation time for both parameter sets as expected by the high activation barrier between Mg^{2+} and phosphate ion (Table 3). The ions bind directly to OP1/OP2 atoms of residues 23 and 24 with an average distance of 1.89 Å with MG^{CHARMM} and 1.95 Å with MG^{NEW}, in agreement with the values seen in the PMFs of the model systems. The distances in the X-ray structure are 2.1−2.4 Å. In addition, these ions have indirect contacts to adjacent atoms, as observed in the X-ray structure. But the MG^{NEW} parameters, on average, have slightly fewer water-bridged contacts per Mg^{2+} (2.4) than MG^{CHARMM} (2.9), in line with the Mg^{2+}−water results (Table 4).

Table 4. Number of Water Bridge Interactions of Mg^{2+} Ions with *add* A-Riboswitch[a]

	MG^{CHARMM}		MG^{NEW}	
RNA atoms	#Mg	contacts/Mg	#Mg	contacts/Mg
all	24.4 ± 2.0	2.6 ± 0.3	22.2 ± 1.8	2.7 ± 0.3
PO	10.8 ± 2.3	2.2 ± 0.4	10.4 ± 1.8	2.3 ± 0.4
SU	0.9 ± 0.8	1.2 ± 0.5	0.9 ± 0.9	1.3 ± 0.5
BA	1.7 ± 1.3	1.7 ± 1.0	1.5 ± 1.1	2.3 ± 0.9
PO + SU	4.9 ± 1.7	3.2 ± 0.6	2.8 ± 1.3	3.3 ± 0.8
PO + BA	4.8 ± 1.5	3.5 ± 0.6	5.9 ± 1.2	3.7 ± 0.5
SU + BA	0.3 ± 0.5	3.1 ± 1.2	0.4 ± 0.5	2.6 ± 1.0
PO + SU + BA	0.9 ± 0.8	3.5 ± 1.5	0.4 ± 0.6	3.6 ± 1.1

[a]PO, SU, and BA refer to the phosphate groups, sugars, and bases, respectively. Standard deviations from the time averages are also reported.

Table 4 shows the time-average number of ions that have at least one water-bridged contact (distances less than 2.4 Å for $Mg-O_W$ and H_W-O/N_{RNA}) with any nitrogen or oxygen atom of the *add* A-riboswitch. Table 4 also reports the average number of water bridged contacts that each $[Mg(H_2O)_6]^{+2}$ complex has with any acceptor atoms. The contacts have been categorized according to which RNA part they are in contact with. Figure 2 shows a selection of indirect Mg^{2+} binding to the *add* A-riboswitch together with free and direct bound ions, as observed in the simulations.

It is evident that the total average number of interacting ions is slightly larger for MG^{CHARMM} (24.4) than for MG^{NEW} (22.2) and that almost half of these ions only interact with the O1P and/or O2P of the phosphate (O3′ and O5′ do not have any contacts at all with Mg^{2+}). For both parameter sets, interactions of Mg^{2+} ions only with the sugar units or the bases are not frequent (~4% and 8% of total interactions). This may be due to the confined space around these parts. Simultaneous interactions with phosphates and base or sugar units are common (Figure 2) and, together, involve almost half of the interacting ions for both the parameter sets. While simultaneous interactions with a sugar and base are very rare, there is on average one Mg^{2+} ion interacting with all three RNA parts simultaneously. The ions that interact with multiple parts of the RNA residues are often deeply buried in the RNA (Figure 2), and each $[Mg(H_2O)_6]^{+2}$ complex is seen having on average three to four (and up to as much as seven to eight on some occasions) contacts with oxygens and nitrogens with both the compared parameter sets. The $[Mg(H_2O)_6]^{+2}$ complexes that interact exclusively with the phosphate groups also form multiple contacts, which is a result of the $[Mg(H_2O)_6]^{+2}$

complex water bridging to O_P's of two adjacent residues (Figure 2).

The average lifetime of the indirect contacts is approximately 65 ps for O_P contacts and 36 ps for sugar and base contacts with only minor differences (<1 ps) between the MG^{CHARMM} and MG^{NEW} parameters. This is considerably longer than predicted from the second shell exchange rates of the model systems (2−5 ps) presented above, which can be explained by the cooperative effect of multiple, simultaneous contacts and the confined space around the ion−water complexes.

CONCLUSIONS

We have evaluated the performance of two Mg^{2+} ion models, implemented in the biomolecular force fields, AMBER99 and CHARMM27, to reproduce the kinetic properties of the binding of Mg^{2+} ions with water and the phosphate ion. Molecular dynamics simulations together with umbrella sampling have been performed to calculate the activation barrier between the cation and water and between the cation and phosphate ion. We then examined the effect of different sets of parameters for Mg^{2+} and three models for the water molecules (TIP3P, SPC/E, and TIP5P). The water exchange rate was calculated from the free energy barrier of water removal, which gave comparable results to the directly counted water exchange rate for the case of Na^+.

For the most biologically abundant cations, such as Na^+, K^+, and Ca^{2+}, the exchange rates are found around 10^{10} to 10^{11} s^{-1} (using MG^{CHARMM}/TIP3P), while Mg^{2+} ions exchange on the order of 10^3 s^{-1}. In particular, the $MG^{LB\text{-}Åqvist}$/TIP3P combination gives the slower exchange rate, while MG^{CHARMM}/TIP5P gives the faster. The trend in exchange rate values for ions is found to be $K^+ > Na^+ > Ca^{2+} > Mg^{2+}$, which agrees with the experimental data by Helm and Merbach.[68] The calculated values lie within an order of magnitude from the experimental values, except for Mg^{2+} ions, where the difference with experimental values ($k = 6.7 \times 10^5$ s^{-1}) is huge. For this ion, the difference between parameter sets or water models is insignificant when compared to the deviations from experimental values.

On the basis of these results, a new set of Mg^{2+} parameters (MG^{NEW}) was developed by fitting to the activation free energy in the Mg^{2+}−water system. The new set reproduces not only the experimental exchange rate but also structural data of the binding of Mg^{2+} ions to the water molecule better than other models.

To model interactions between Mg^{2+} and an RNA backbone phosphate group, we used a system with a Mg^{2+} cation and a monophosphate anion (dimethylphosphate) in explicit solvent. The results show that exchange between metal ion and phosphate ion is faster with MG^{NEW}/TIP3P (10.3 s^{-1}) than with MG^{CHARMM} (4.1×10^{-1} and 2.6×10^{-3} s^{-1} for TIP5P and TIP3P respectively) or with $MG^{LB\text{-}Åqvist}$/TIP3P (1.3×10^{-3} s^{-1}). No experimental data are available for the ion exchange for this specific system, but NMR data for nucleic acid systems indicate an exchange rate of $(0.50–3.0) \times 10^3$ s^{-1}, close to MG^{NEW}/TIP3P. From a structural point of view, the results from MG^{NEW}/TIP3P have better agreement with the X-ray diffraction data of Caminiti[72] than the other models.

Finally, the MG^{NEW}/TIP3P model was applied in a biological context (with the *add* A-riboswitch) and compared with MG^{CHARMM}/TIP3P. The Mg^{2+} ions parameters do not affect the main structure feature of the RNA system. Both parameter sets reproduce the ion direct binding to RNA in agreement with the X-ray structure.[47] Concerning the indirect binding, an average number of 22−24 Mg^{2+} ions interact with the RNA (one Mg^{2+} ion each three residues) with an average residence time of 51−53 ps. No differences were observed between the parameter sets concerning the type of RNA atoms that are water bridged with the magnesium ions. A 9% decrease in the average number of the indirect Mg^{2+}−RNA contacts are observed with MG^{NEW}/TIP3P model.

Together, these results provide support for the ability of the newly developed parameters to improve the kinetic description of Mg^{2+} in water solution and to be used in nucleic acid simulation in combination with the CHARMM force field. With simulations now being performed on the millisecond scale,[74,75] the correct representation of slow processes is becoming more important. A good description of the kinetic properties of the magnesium ion−water is the first step toward an atomistic force field able to simulate the kinetic step of RNA systems accurately. The following natural step will be to evaluate/improve the kinetic description of Mg^{2+} phosphate interactions, but first more system-specific experimental data are necessary.

AUTHOR INFORMATION

Corresponding Author

*E-mail: alessandra.villa@ki.se.

Notes

The authors declare no competing financial interest.

ACKNOWLEDGMENTS

The authors are grateful to the Swedish Research Council for financial support.

REFERENCES

(1) Woodson, S. A. *Curr. Opin. Chem. Biol.* **2005**, *9*, 104−109.
(2) Pyle, A. M. *J. Biol. Inorg. Chem.* **2002**, *7*, 679−690.
(3) Draper, D. E.; Grilley, D.; Soto, A. M. *Annu. Rev. Biophys. Biomol.* **2005**, *34*, 221−243.
(4) Klein, D. J.; Moore, P. B.; Steitz, T. A. *RNA* **2004**, *10*, 1366−1379.
(5) Draper, D. E. *RNA* **2004**, *10*, 335−343.
(6) Fang, X. W.; Pan, T.; Sosnick, T. R. *Nat. Struct. Biol.* **1999**, *6*, 1091−1095.
(7) Fang, X. W.; Thiyagarajan, P.; Sosnick, T. R.; Pan, T. *Proc. Natl. Acad. Sci. U. S. A.* **2002**, *99*, 8518−8523.
(8) Leroy, J. L.; Gueron, M.; Thomas, G.; Favre, A. *Eur. J. Biochem.* **1977**, *74*, 567−574.
(9) Draper, D. E. *Biophys. J.* **2008**, *95*, 5489−5495.
(10) Stein, A.; Crothers, D. M. *Biochemistry* **1976**, *15*, 160−168.
(11) Romer, R.; Hach, R. *Eur. J. Biochem.* **1975**, *55*, 271−284.
(12) Caminiti, R.; Licheri, G.; Piccaluga, G.; Pinna, G. *J. Appl. Crystallogr.* **1979**, *12*, 34−38.
(13) Palinkas, G.; Radnai, T.; Dietz, W.; Szasz, G. I.; Heinzinger, K. *Z. Naturforsch. A* **1982**, *37*, 1049−1060.
(14) Soto, A. M.; Misra, V.; Draper, D. E. *Biochemistry* **2007**, *46*, 2973−2983.
(15) Leipply, D.; Draper, D. E. *J. Am. Chem. Soc.* **2011**, *133*, 13397−13405.
(16) Auffinger, P.; Westhof, E. *J. Mol. Biol.* **2000**, *300*, 1113−1131.
(17) Erat, M. C.; Sigel, R. K. *Met. Ions Life Sci.* **2011**, *9*, 37−100.
(18) Cate, J. H.; Gooding, A. R.; Podell, E.; Zhou, K. H.; Golden, B. L.; Kundrot, C. E.; Cech, T. R.; Doudna, J. A. *Science* **1996**, *273*, 1678−1685.
(19) Black, C. B.; Huang, H. W.; Cowan, J. A. *Coord. Chem. Rev.* **1994**, *135*, 165−202.
(20) Cowan, J. A. *J. Am. Chem. Soc.* **1991**, *113*, 675−676.

(21) Cowan, J. A.; Huang, H. W.; Hsu, L. Y. *J. Inorg. Biochem.* **1993**, *52*, 121−129.
(22) Pabit, S. A.; Meisburger, S. P.; Li, L.; Blose, J. M.; Jones, C. D.; Pollack, L. *J. Am. Chem. Soc.* **2010**, *132*, 16334−16336.
(23) Fiala, R.; Spackova, N.; Foldynova-Trantirkova, S.; Sponer, J.; Sklenar, V.; Trantirek, L. *J. Am. Chem. Soc.* **2011**, *133*, 13790−3.
(24) Misra, V. K.; Draper, D. E. *J. Mol. Biol.* **2002**, *317*, 507−21.
(25) Tan, Z. J.; Chen, S. J. *Biophys. J.* **2010**, *99*, 1565−76.
(26) Gresh, N.; Sponer, J. E.; Spackova, N.; Leszczynski, J.; Sponer, J. *J. Phys. Chem. B* **2003**, *107*, 8669−8681.
(27) Oliva, R.; Cavallo, L. *J. Phys. Chem. B* **2009**, *113*, 15670−15678.
(28) Chen, A. A.; Marucho, M.; Baker, N. A.; Pappu, R. V.; Daniel, H. In *Biophysical, Chemical, and Functional Probes of RNA Structure, Interactions and Folding: Part B*; Academic Press New York: 2009; Chapter 20 - Simulations of RNA Interactions with Monovalent Ions, pp 411−432.
(29) MacKerell, A. D. *J. Phys. Chem. B* **1997**, *101*, 646−650.
(30) Mocci, F.; Laaksonen, A.; Lyubartsev, A.; Saba, G. *J. Phys. Chem. B* **2004**, *108*, 16295−16302.
(31) Singh, A.; Sethaphong, L.; Yingling, Y. G. *Biophys. J.* **2011**, *101*, 727−735.
(32) Neely, J.; Connick, R. *J. Am. Chem. Soc.* **1970**, *92*, 3476−&.
(33) Bleuzen, A.; Pittet, P. A.; Helm, L.; Merbach, A. E. *Magn. Reson. Chem.* **1997**, *35*, 765−773.
(34) Åqvist, J. *J. Phys. Chem.* **1990**, *94*, 8021−8024.
(35) Jiao, D.; King, C.; Grossfield, A.; Darden, T. A.; Ren, P. Y. *J. Phys. Chem. B* **2006**, *110*, 18553−18559.
(36) Yu, H. B.; Whitfield, T. W.; Harder, E.; Lamoureux, G.; Vorobyov, I.; Anisimov, V. M.; MacKerell, A. D.; Roux, B. *J. Chem. Theory Comput.* **2010**, *6*, 774−786.
(37) Kastenholz, M. A.; Hunenberger, P. H. *J. Chem. Phys.* **2006**, *124*, 224501.
(38) Kastenholz, M. A.; Hunenberger, P. H. *J. Chem. Phys.* **2006**, *124*, 124106.
(39) Cornell, W. D.; Cieplak, P.; Bayly, C. I.; Gould, I. R.; Merz, K. M.; Ferguson, D. M.; Spellmeyer, D. C.; Fox, T.; Caldwell, J. W.; Kollman, P. A. *J. Am. Chem. Soc.* **1995**, *117*, 5179−5197.
(40) Wang, J. M.; Cieplak, P.; Kollman, P. A. *J. Comput. Chem.* **2000**, *21*, 1049−1074.
(41) MacKerell, A. D.; Banavali, N. K. *J. Comput. Chem.* **2000**, *21*, 105−120.
(42) Foloppe, N.; MacKerell, A. D. *J. Comput. Chem.* **2000**, *21*, 86−104.
(43) Cowan, J. A. *Inorg. Chem.* **1991**, *30*, 2740−2747.
(44) Jorgensen, W. L.; Chandrasekhar, J.; Madura, J.; Impey, R. W.; Klein, M. L. *J. Chem. Phys.* **1983**, *79*, 926−935.
(45) Berendsen, H. J. C.; Grigera, J. R.; Straatsma, T. P. *J. Phys. Chem.* **1987**, *91*, 6269−6271.
(46) Mahoney, M. W.; Jorgensen, W. L. *J. Chem. Phys.* **2000**, *112*, 8910−8922.
(47) Serganov, A.; Yuan, Y. R.; Pikovskaya, O.; Polonskaia, A.; Malinina, L.; Phan, A. T.; Hobartner, C.; Micura, R.; Breaker, R. R.; Patel, D. J. *Chem. Biol.* **2004**, *11*, 1729−1741.
(48) Serganov, A. *RNA Biol.* **2010**, *7*, 98−103.
(49) Leipply, D.; Draper, D. E. *Biochemistry* **2011**, *50*, 2790−2799.
(50) Lemay, J. F.; Penedo, J. C.; Tremblay, R.; Lilley, D. M. J.; Lafontaine, D. A. *Chem. Biol.* **2006**, *13*, 857−868.
(51) Noeske, J.; Schwalbe, H.; Wohnert, J. *Nucleic Acids Res.* **2007**, *35*, 5262−5273.
(52) Denning, E. J.; Priyakumar, U. D.; Nilsson, L.; Mackerell, A. D. *J. Comput. Chem.* **2011**, *32*, 1929−1943.
(53) Berman, H. M.; Westbrook, J.; Feng, Z.; Gilliland, G.; Bhat, T. N.; Weissig, H.; Shindyalov, I. N.; Bourne, P. E. *Nucleic Acids Res.* **2000**, *28*, 235−242.
(54) Brünger, A. T.; Karplus, M. *Proteins* **1988**, *4*, 148−156.
(55) Brooks, B. R.; Brooks, C. L.; Mackerell, A. D.; Nilsson, L.; Petrella, R. J.; Roux, B.; Won, Y.; Archontis, G.; Bartels, C.; Boresch, S.; Caflisch, A.; Caves, L.; Cui, Q.; Dinner, A. R.; Feig, M.; Fischer, S.; Gao, J.; Hodoscek, M.; Im, W.; Kuczera, K.; Lazaridis, T.; Ma, J.; Ovchinnikov, V.; Paci, E.; Pastor, R. W.; Post, C. B.; Pu, J. Z.; Schaefer, M.; Tidor, B.; Venable, R. M.; Woodcock, H. L.; Wu, X.; Yang, W.; York, D. M.; Karplus, M. *J. Comput. Chem.* **2009**, *30*, 1545−1614.
(56) Brooks, B. R.; Bruccoleri, R. E.; Olafson, B. D.; States, D. J.; Swaminathan, S.; Karplus, M. *J. Comput. Chem.* **1983**, *4*, 187−217.
(57) Nilsson, L. *J. Comput. Chem.* **2009**, *30*, 1490−1498.
(58) Ryckaert, J.-P.; Ciccotti, G.; Berendsen, H. J. C. *J. Comput. Phys.* **1977**, *23*, 327−341.
(59) Darden, T.; York, D.; Pedersen, L. *J. Chem. Phys.* **1993**, *98*, 10089−10092.
(60) Essmann, U.; Perera, L.; Berkowitz, M. L.; Darden, T.; Lee, H.; Pedersen, L. G. *J. Chem. Phys.* **1995**, *103*, 8577−8593.
(61) Berendsen, H. J. C.; Postma, J. P. M; van Gunsteren, W. F.; Dinola, A.; Haak, J. R. *J. Chem. Phys.* **1984**, *81*, 3684−3690.
(62) Allner, O.; Nilsson, L. *RNA* **2011**, *17*, 2177−2188.
(63) Boczko, E. M.; Brooks, C. L. *J. Phys. Chem.* **1993**, *97*, 4509−4513.
(64) Kumar, S.; Bouzida, D.; Swendsen, R. H.; Kollman, P. A.; Rosenberg, J. M. *J. Comput. Chem.* **1992**, *13*, 1011−1021.
(65) Tobias, D. J.; Brooks, C. L. *Chem. Phys. Lett.* **1987**, *142*, 472−476.
(66) Fleischman, S. H.; Brooks, C. L. *J. Chem. Phys.* **1987**, *87*, 3029−3037.
(67) Ohtaki, H.; Radnai, T. *Chem Rev* **1993**, *93*, 1157−1204.
(68) Helm, L.; Merbach, A. E. *Chem Rev* **2005**, *105*, 1923−1959.
(69) MacKerell, A. Mg parameters from the CHARMM 22 FF. Available from http://mackerell.umaryland.edu/CHARMM_ff_params.html (accessed March 05, 2012).
(70) Schmid, R.; Miah, A. M.; Sapunov, V. N. *Phys. Chem. Chem. Phys.* **2000**, *2*, 97−102.
(71) Marcus, Y. *J. Chem. Soc., Faraday Trans.* **1991**, *87*, 2995−2999.
(72) Caminiti, R. *J. Mol. Liq.* **1984**, *28*, 191−204.
(73) Priyakumar, U. D.; MacKerell, A. D. *J. Mol. Biol.* **2010**, *396*, 1422−1438.
(74) Dror, R. O.; Jensen, M. O.; Borhani, D. W.; Shaw, D. E. *J. Gen. Physiol.* **2010**, *135*, 555−562.
(75) Shaw, D. E.; Maragakis, P.; Lindorff-Larsen, K.; Piana, S.; Dror, R. O.; Eastwood, M. P.; Bank, J. A.; Jumper, J. M.; Salmon, J. K.; Shan, Y. B.; Wriggers, W. *Science* **2010**, *330*, 341−346.
(76) Weingartner, H.; Muller, K. J.; Hertz, H. G.; Edge, A. V. J.; Mills, R. *J. Phys. Chem.* **1984**, *88*, 2173−2178.